*Journal of The Electrochemical Society*, **158** (5) E45-E49 (2011)
0013-4651/2011/158(5)/E45/5/$28.00 © The Electrochemical Society


# Electrochemical Reduction of $CO_2$ to $CH_3OH$ at Copper Oxide Surfaces

**M. Le,[a,b] M. Ren,[a,b] Z. Zhang,[c] P. T. Sprunger,[b,c] R. L. Kurtz,[b,c] and J. C. Flake[a,b,*,z]**

[a]*Gordon and Mary Cain Department of Chemical Engineering,* [b]*Energy Frontier Research Center, and* [c]*Department of Physics and Astronomy, Louisiana State University, Baton Rouge, Louisiana 70803, USA*

The direct reduction of $CO_2$ to $CH_3OH$ is known to occur at several types of electrocatalysts including oxidized Cu electrodes. In this work, we examine the yield behavior of an electrodeposited cuprous oxide thin film and explore relationships between surface chemistry and reaction behavior relative to air-oxidized and anodized Cu electrodes. $CH_3OH$ yields (43 μmol $cm^{-2}$ $h^{-1}$) and Faradaic efficiencies (38%) observed at cuprous oxide electrodes were remarkably higher than air-oxidized or anodized Cu electrodes suggesting Cu(I) species may play a critical role in selectivity to $CH_3OH$. Experimental results also show $CH_3OH$ yields are dynamic and the copper oxides are reduced to metallic Cu in a simultaneous process. Yield behavior is discussed in comparison with photoelectrochemical and hydrogenation reactions where the improved stability of Cu(I) species may allow continuous $CH_3OH$ generation.
 [DOI: 10.1149/1.3561636] 

Manuscript submitted January 13, 2011; revised manuscript received February 4, 2011. Published March 25, 2011. This was Paper 301 presented at the Las Vegas, Nevada, Meeting of the Society, October 10–15, 2010.

The direct electrochemical reduction of $CO_2$ to $CH_3OH$ presents an attractive method to produce liquid fuels such as dimethyl ether (DME), synthetic gasoline,[1,2] and feedstocks for several organic compounds. Although $CH_3OH$ is typically produced in hydrogenation reactions using syngas and $CO_2$ feeds (400–800 K, 2–12 MPa),[3–8] the aqueous electrochemical process operates at room temperature and offers a convenient method to store electrical energy without increasing $CO_2$ emissions. As described by Hori, electrochemical product selectivity and efficiency of $CO_2$ reduction reactions are highly dependent on the electrocatalysts and operating conditions.[9] Direct $CO_2$ to $CH_3OH$ electrochemical reduction reactions in aqueous electrolytes were first reported by Frese et al. using III–V semiconductor electrodes (GaAs and InP); however, maximum current densities were lower than 1 mA $cm^{-2}$.[10] Similar works have also demonstrated $CH_3OH$ as a direct product of electrochemical $CO_2$ reduction reactions on Mo,[11] and several types of Ru electrodes[12–16] at current densities less than 2 mA $cm^{-2}$ with Faradaic efficiencies up to 60%. At present, the greatest reported current densities and Faradaic efficiencies towards $CH_3OH$ production are associated with oxidized Cu electrodes with current densities up to 33 mA $cm^{-2}$ and Faradaic efficiencies greater than 100%.[17] It is important to note Faradaic efficiencies are based on a six-electron reduction reaction and efficiencies greater than unity indicate electrochemical–chemical (EC or CE) mechanisms.[9,17,18] While copper oxides show the greatest yields and efficiencies, a more fundamental question regarding oxidized Cu electrodes centers on their formal reduction potentials relative to $CO_2$. The formal potential for $CO_2$ reduction to $CH_3OH$ occurs 20 mV positive of the SHE, while copper oxides are reduced at more positive potentials. Further, several $CO_2$ reduction studies propose an initial step requiring CO which has a formal potential of –0.103 V (SHE)[9,18–25]

$$CO_2 + 6H^+ + 6e^- \rightleftharpoons CH_3OH + H_2O \quad E_0 = 0.020 \text{ V vs SHE} \quad [1]$$

$$CO_2 + 2H^+ + 2e^- \rightleftharpoons CO + H_2O \quad E_0 = -0.103 \text{ V vs SHE} \quad [2]$$

$$Cu_2O + 2H^+ + 2e^- \rightleftharpoons 2Cu + H_2O \quad E_0 = -0.052 \text{ V vs SHE} \quad [3]$$

$$CuO + 2H^+ + 2e^- \rightleftharpoons Cu + H_2O \quad E_0 = -0.127 \text{ V vs SHE} \quad [4]$$

$$2CuO + 2H^+ + 2e^- \rightleftharpoons Cu_2O + H_2O \quad E_0 = -0.197 \text{ V vs SHE} \quad [5]$$

Although the oxidation states and electrode stability were not explicitly considered in previous electrocatalytic reduction studies, copper oxide catalysts are known to favor $CH_3OH$ in both photoelectrochemical and hydrogenation systems. Photoelectrochemical $CO_2$ reduction reactions are typically performed on Cu-loaded titania surfaces; however, quantum efficiencies for $CO_2$ reduction under UV or solar radiation conditions are typically very low.[26,27] As with Cu-based electrodes, $CH_3OH$ formation at photoelectrodes is associated with oxidized Cu species, particularly Cu/Cu(I) interfaces.[28,29] Likewise, several works suggest copper oxides, Cu cations, or oxide interfaces provide active reduction sites and ZnO stabilizes oxidized Cu in hydrogenation reactions.[8,30,31] In this work, we examine the surface chemistry and $CH_3OH$ formation behavior of several electrocatalysts with Cu(I) surface sites and consider the possible pathways for the direct electrochemical reduction of $CO_2$ to $CH_3OH$.

## Experimental

Electrodes for $CO_2$ reduction were fabricated via oxidization of Cu foils (99.99%, ESPI Metals) or thin film electrodeposition. Air-oxidized electrodes were prepared by first cleaning the foil in 0.1 M hydrochloric acid (HCl) (36.5–38.0%, Sigma–Aldrich) for 20 s followed by oxidation in an air furnace at 403 K for 17 h. Anodized electrodes were created by electrochemically oxidizing Cu foil in 0.5 M potassium bicarbonate ($KHCO_3$) (99.7%, Sigma–Aldrich) at a constant potential of 1.25 V (SCE) for 3 min. Cuprous oxide thin films ($Cu_2O$) were electrodeposited on stainless steel substrates at –0.555 V (SCE) and 333 K for 30 min in a lactate solution including 0.4 M copper sulfate ($CuSO_4$) (>99%, Sigma–Aldrich) and 3 M lactic acid (Sigma–Aldrich) at *p*H 9.0 with Cu foil as the anode.[32,33] All electrodes were rinsed with deionized water and dried under $N_2$ before use as cathodes. An Ag/AgCl electrode saturated with NaCl was selected as the reference electrode along with a Pt wire as the counter electrode. A Princeton Applied Research Model 263A potentiostat was used in all electrochemical experiments.

$CO_2$ reduction experiments were performed in a typical three-electrode cell (30 mL volume) at potentials ranging from –1.0 to –1.9 V (SCE). Typical cathode areas ranged from 1.0 to 2.0 $cm^2$. An aqueous electrolyte (0.5 M $KHCO_3$) was saturated with ultrapure $CO_2$ (99.9999%, Airgas, USA) by bubbling for 30 min (298 K, *p*H 7.6). Faradaic efficiencies were calculated assuming six electrons are required per $CH_3OH$ molecule. Liquid phase samples were taken from the sealed reactor via a syringe septum and reaction products were analyzed by Gas Chromatography-Flame Ionization Detector (GC-FID) (Agilent, GC5890). Electrolytes were purified prior to the reaction by pre-electrolysis at 0.025 mA $cm^{-2}$ for 24 h with Pt wires as both cathode and anode.[34] Before pre-electrolysis, $Zn^{2+}$ concentrations were approximately 0.2 ppm and $Fe^{2+}$ concentrations were less than 0.02 ppm as determined by Inductively Coupled Plasma -

* Electrochemical Society Active Member.
z E-mail: johnflake@lsu.edu

Mass Spectrometry (ICP-MS). After pre-electrolysis, ion contamination levels were below detectable limits (0.02 ppm).

The electrochemical behavior of copper oxide electrodes were evaluated using cyclic voltammetry at a scan rate of 10 mV $s^{-1}$ in the same $CO_2$ saturated 0.5 M $KHCO_3$ electrolyte used in reduction studies. Microstructure and morphology were analyzed using Hitachi S-3600N Variable Pressure Scanning Electron Microscope (VP-SEM). Near-Edge x-ray absorption fine structure (NEXAFS) measurements were performed at the LSU Center for Advanced Microstructures and Devices (CAMD) synchrotron's varied-line-space plane-grating-monochromator (VLSPGM) beamline. The photon energy scale was calibrated with Cu standard samples (CuO, Cu and $Cu_2O$). The incident beam intensity was concurrently monitored by an Au mesh placed in the incident beam before sample. The measured sample spectrum $I_0$ (total electron yield mode) was normalized by the total electron yield of the Au mesh. Reproducibility of the spectra was carefully monitored and verified by multiple scanning (typically four times). NEXAFS spectra were acquired at room temperature at both the O K-edge and the Cu L-edge regions. Auger electron spectra were obtained using an Ultra-high Vacuum x-ray photoelectron spectroscopy (UHV XPS) (PHI 5100) at the Major Analytical Instrumentation Center (MAIC) at University of Florida including sputter depth profiling. Crystal orientations of copper oxides were analyzed by x-ray Diffraction (XRD) using a Cr-Kα (λ = 2.291 Å) source at a scanning rate of 3° $min^{-1}$.

## Results and Discussion

As shown in Fig. 1, $CH_3OH$ formation rates at electrodeposited cuprous oxide electrodes are quite high ranging from 10 to 43 μmol $cm^{-2}$ $h^{-1}$; yields from anodized Cu electrodes ranged from 0.9 to 1.5 μmol $cm^{-2}$ $h^{-1}$; and yields from air-oxidized Cu electrodes ranged from 0.08 to 0.9 μmol $cm^{-2}$ $h^{-1}$ (all based on geometric electrode areas). Formation rates typically increase with potential from –1.1 V (SCE) and reach a maxima near –1.55 V (SCE), then decrease dramatically at potentials more cathodic than –1.55 V (SCE) accompanied with significant hydrogen evolution. Figure 2 shows electrodeposited cuprous oxide electrodes allow significantly higher Faradaic effeciencies relative to anodized Cu and air-oxidized Cu electrodes. The greatest Faradaic efficiency (38%) was also observed using electrodeposited cuprous oxide electrodes at –1.1 V (SCE). No liquid phase products other than $CH_3OH$ were detected and gas phase analysis showed predominantly $H_2$ and trace amounts of CO.

Initial experiments also showed product distribution is dynamic at all oxidized Cu electrodes; $CH_3OH$ formation rates tend to diminish at longer reaction times (>30 min) and are accompanied with

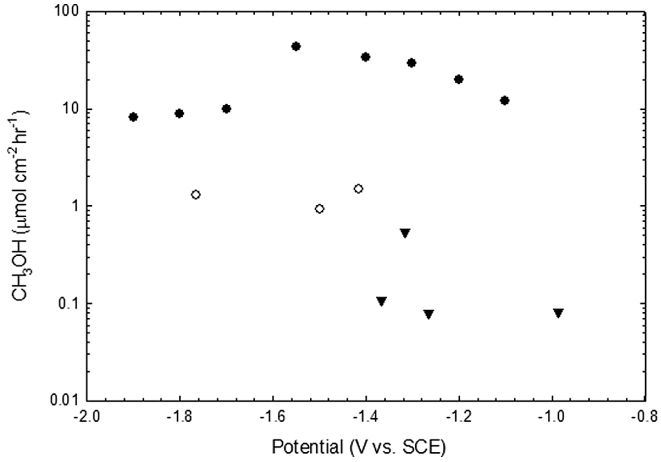


**Figure 1.** $CH_3OH$ formation rate vs potential of ▼, air-oxidized Cu; ○, anodized Cu; •, electrodeposited cuprous oxide film.

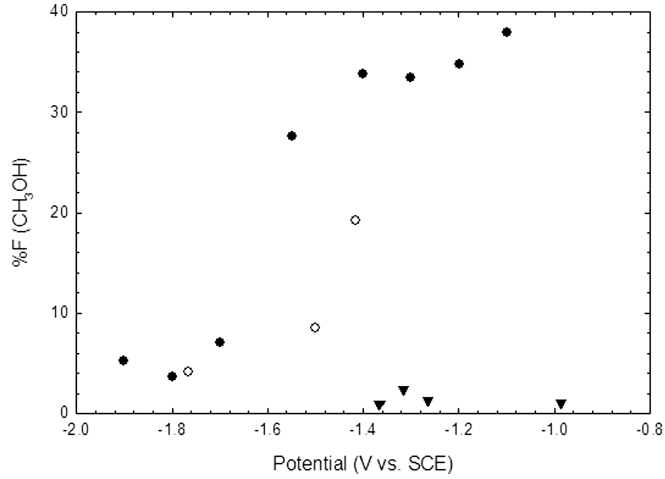


**Figure 2.** Faradaic efficiencies vs potential of ▼, air-oxidized Cu; ○, anodized Cu; •, electrodeposited cuprous oxide film.

$CH_4$ generation. As described by Hori, $CH_4$ is the primary reduction product at Cu electrodes which suggests these oxides are reduced during the reaction. In this case, a potential of –1.5V (SCE) was used with a batch reaction time of 10 min to maximize product detectability without significant loss in activity. While the primary loss of activity may be associated with reduction of the active copper oxides, losses may also be affectd by contamination from the impurities in the electrolyte or $CH_3OH$ oxidation at counter electrode.[9]

In efforts to understand the dynamic reaction behavior at copper oxide electrodes, we examined the surface morphology, composition and structure of the electrodes before and after 10 min reduction reactions. Figure 3 shows SEM images of the electrodes before and after the 10 min $CO_2$ reduction reaction at –1.5 V (SCE). Dispersed crystallites approximately 1 μm in size with 2 μm spacing are seen on the air-oxidized Cu electrode in Fig. 3a. The microcrystals are absent after the 10 min reaction at –1.5 V (SCE) as shown in Fig. 3b. As seen in Fig. 3c, anodized Cu electrodes show a porous layer (approximately 200 nm thick) with copper oxide nodules approximately 2 μm in diameter before the reaction and smaller nodules after the reaction as seen in Fig. 3d. Figure 3e reveals electrodeposited cuprous oxide crystals with well-defined four-sided pyramid geometry with a strong (100) orientation; crystal dimensions are approximately 2 μm on edge and the film is approximately 2 μm thick. As with the anodized electrode, average crystal dimensions are reduced to less than 1 μm after the reaction as shown in Fig. 3f.

$CH_3OH$ yields from the cuprous oxide thin film electrodes are remarkable, at least one order of magnitude greater than the anodized electrode and two orders of magnitude greater than the air-oxidized electrode based on apparent (geometric) electrode area. Actual areas of the electrodes relative to the apparent areas were estimated as 1.3× greater for the air-oxidized sample, 3.0× greater for the anodized sample and 1.7× greater for the cuprous oxide film based on SEM analysis. If yields are normalized to actual (estimated) surface areas, the anodized Cu yield results are comparable to the air-oxidized electrode while yields from the cuprous oxide film remain approximately two orders of magnitude greater than either the air-oxidized or anodized electrodes. The dramatic increase in $CH_3OH$ yields associated with the cuprous oxide thin film suggests Cu(I) species may play a key role in reducing $CO_2$ to $CH_3OH$.

Cu L-edge NEXAFS spectra of the air-oxidized, the anodized, and electrodeposited samples, before and after the 10 min reaction at –1.5 V (SCE) are shown in Fig. 4, along with three standards: Cu(0), Cu(I), and Cu(II). The CuO standard is characterized by two relatively intense features at 930.5 and 950.5 eV. They arise from the dipole transitions of the Cu $2p_{3/2}$ ($L_{III}$) and Cu $2p_{1/2}$ ($L_{II}$) into

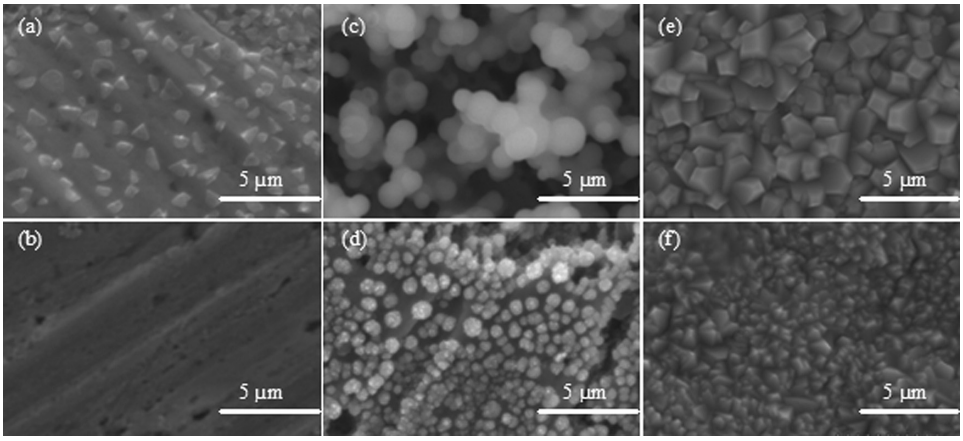


**Figure 3.** SEM images of (a), air-oxidized Cu before reaction; (b), after reaction; (c), anodized Cu before reaction; (d), after reaction; (e), electrodeposited cuprous oxide film before reaction; (f), after reaction.

the empty d-states. The smaller peak at ∼938 eV is a shake-up (multielectron excitation) satellite. Similarly, the Cu and $Cu_2O$ standards show intense features at ∼933 and ∼953.5 eV, indicating Cu(0) and/or Cu(I) with differing satellite structure. As seen in Fig. 5, the air-oxidized Cu and electrodeposited cuprous oxide film shows a Cu(I) peak at 933.3 eV, with a similar satellite structure as compared with the $Cu_2O$ standard. This peak decreases intensity after the $CO_2$ reduction reaction. Oxide reduction is also confirmed by the O–K edge of air-oxidized Cu and electrodeposited cuprous oxide films with a peak at 533.5 eV and similar satellite structure as $Cu_2O$ standard as shown in Fig. 5. As for anodized Cu, the $L_{III}$ peak at 930.3 eV attenuates upon reaction and the Cu(I) at 933.3 eV decreases as metallic Cu(0) appears at 933 eV. The O–K edge of the anodized Cu shows a small shoulder at ∼530.8 eV and extends to a peak at ∼534.5 eV suggesting the anodized Cu electrode surface includes a mixture of CuO, $Cu_2O$ and $Cu_4O_3$.[35]

Auger spectra are shown in Fig. 6 before and after the 10 min reduction reaction at –1.5 V (SCE). The electrodes were sputter cleaned using $Ar^+$ to remove organic contamination prior to analysis. Results for the air-oxidized electrode show a Cu(I) peak at 917.5 eV prior to the reduction reaction and a well defined Cu(0) peak at 919 eV after the reaction. Likewise, the anodized Cu sample

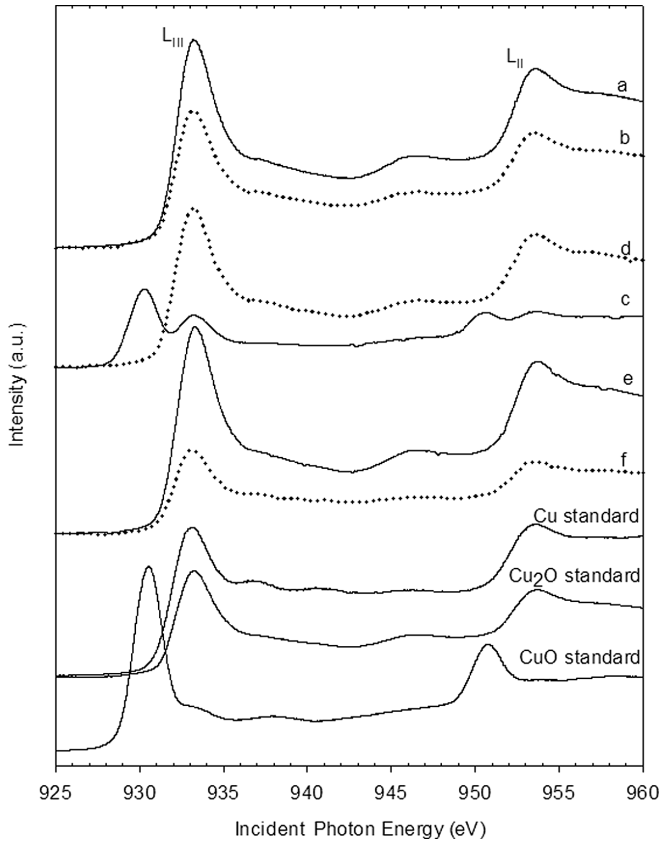


**Figure 4.** NEXAFS spectra of Cu L-edge regions of (a), air-oxidized Cu before reaction; (b), after reaction; (c) anodized Cu before reaction; (d), after reaction; (e), electrodeposited cuprous oxide film before reaction; (f), after reaction.

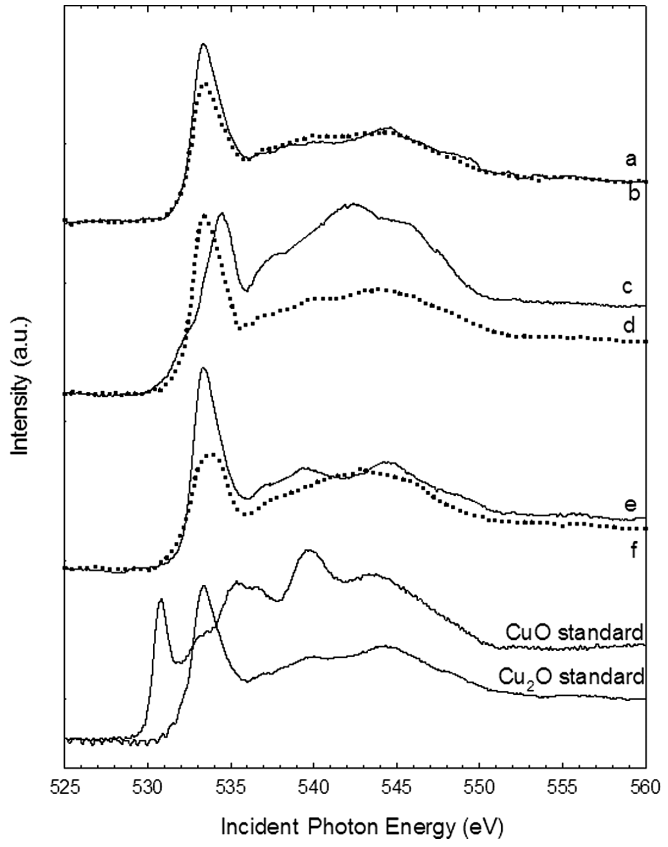


**Figure 5.** NEXAFS spectra of O K-edge regions of (a), air-oxidized Cu before reaction; (b), after reaction; (c) anodized Cu before reaction; (d), after reaction; (e), electrodeposited cuprous oxide film before reaction; (f), after reaction.

shows a broad peak at 918 eV before the reaction and a Cu(0) peak at 919 eV after the reaction. The electrodeposited cuprous oxide film shows a dominant Cu(I) peak at 917.5 eV before the reaction with a small Cu(0) shoulder at 919 eV. Auger spectra of the electrodeposited cuprous oxide sample after the reaction was inconclusive due to delamination from the support.

Qualitatively, $CH_3OH$ yield trends follow Cu(I) intensities prior to the reaction as determined by NEXAFS and Auger analysis. Electrodeposited cuprous oxide films showed $CH_3OH$ formation rates up to 43 μmol $cm^{-2}$ $h^{-1}$ and Faradaic efficiencies up to 38%, while air-oxidized and anodized electrodes showed rates at least one order of magnitude lower. Both Auger and NEXAFS data indicate all oxides electrodes are partially reduced during the 10 min reaction at –1.5 V (SCE), which is consistent with the observation of decreased $CH_3OH$ yields and the simultaneous increase in $CH_4$ production in longer experiments (>30 min). The results suggest $CH_3OH$ production may be primarily associated with Cu(I) surface species which appear to be reduced in a simultaneous process.

Cyclic voltammetry shows oxide reduction behavior depends on the method of preparation. As seen in Fig. 7, the anodized Cu electrode shows a significant increase in cathodic current at near –0.7 V (SCE) which diminishes on the reverse scan. Several large reduction peaks from –1.0 to –2.0 V (SCE) overlapping in the anodized Cu scan suggest copper oxides created in this method are relatively easy to reduce at potentials positive of $CO_2$ reduction. Voltammetric behavior of the air-oxidized Cu and electrodeposited cuprous oxide film shows relatively little hysteresis with an onset reduction potential near –1.2 (SCE) and –1.0 V (SCE) respectively. This behavior indicates the air-oxidized and cuprous oxide film may be relatively more stable in these electrolytes. Further, while both cuprous and cupric oxides are p-type semiconductors ($E_g = 2.1$, 1.2 eV respectively) voltammetric analysis did not show any measurable photocurrents under UV or laboratory lighting. The lack of any appreciable photocurrents suggests surfaces are non-homogeneous (including metallic Cu) or include high levels of defects which cause degenerate/metallic behavior.

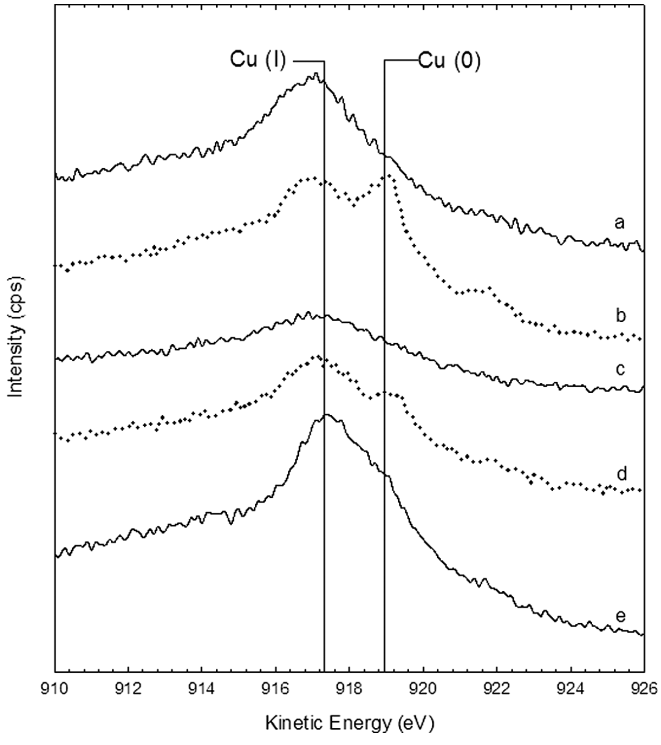


**Figure 6.** Auger spectra (a), air-oxidized Cu before reaction, and (b), after reaction; (c) anodized Cu before reaction, and (d), after reaction; (e), electrodeposited cuprous oxide film before reaction.

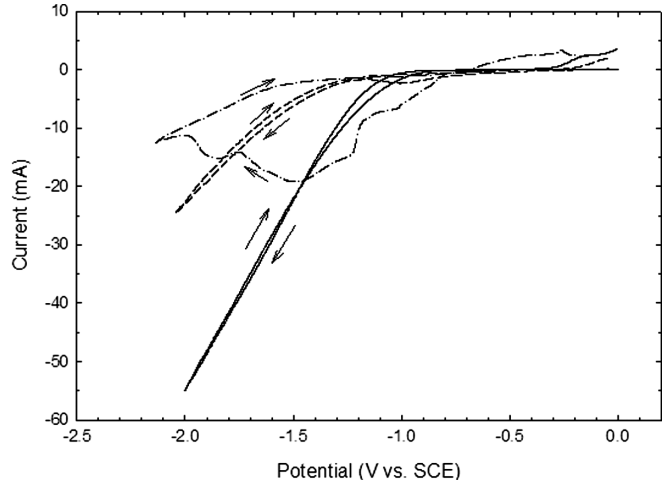


**Figure 7.** Cyclic voltammetry of – –, air-oxidized Cu; –·–·–, anodized Cu; –, electrodeposited cuprous oxide film.

Cu(I) active sites have been proposed in several electrochemical, photoelectrochemical and chemical routes.[3–8,17,26–29] Frese suggests the oxides at the surfaces of GaAs, InP, and Mo in aqueous solutions act in a similar fashion as the Cu(I) species allowing improved CO adsorption and may also affect selectivity to $CH_3OH$. Based on the voltage independence of $CH_3OH$ rates and Faradaic efficiencies greater than unity, the author also suggests an initial chemical (non-faradaic) step involving the formation of adsorbed CO and $O^-$ species. Cu(I) sites were considered to allow the valance band electrons to participate in CO adsorption and formyl (HCO) species are presumably formed by the dissociation of water followed by hydrogenation via adsorbed hydrogen. Unfortunately, the nature of the selectivity to $CH_3OH$ rather than $CH_4$ at copper oxides was not explicitly considered and hydrogen dissociation at metallic Cu is known to be relatively slow.[31,36,37]

Although there is no general consensus on the mechanism for hydrogenation at Cu/ZnO catalysts, Cu(I) sites are thought to promote catalytic activity and selectivity toward $CH_3OH$.[4–6,36–42] While Cu–Zn alloys are considered active sites for $CO_2$ reduction, Cu(I) sites are considered key species for CO adsorption in hydrogenation reactions.[39] Further, Cu(I) sites are believed to stabilize reaction intermediates such as carbonates ($CO_3^{2-}$), formates ($HCOO^-$) and methoxy adsorbates ($H_3CO^-$) due to their higher heats of adsorption.[38] Further, Cu/ZnO hydrogenation catalysts rely on the addition of oxidizers ($H_2O$, $O_2$, and $CO_2$) to retain Cu(I) sites and promote CO adsorption by decreasing the reduction potential of the $CO/H_2$ feed.[39–42] Sheffer et al. showed alkali metals help stabilize Cu(I) active sites and increase Cu(I) concentrations which significantly improve $CH_3OH$ yield.[37] Similarly, Cu(I) species are considered as the active sites in $CH_3OH$ oxidation reactions at copper oxide surfaces. Oxidation studies at single crystal Cu(I) shows $H_3CO$ adsorbed at (111) surfaces (with Cu(I) atoms at the second atomic layer) allows coordinately unsaturated oxygen anions to act as hydrogen abstraction sites for dehydrogenation.[43] In this case, it is possible the unsaturated oxygen atoms at the (111) surfaces of the cuprous oxide film (Fig. 3) act as a hydrogen donors sites in the reduction reaction.

A recent theoretical report by Peterson et al. describes a pathway for the electrochemical reduction of $CO_2$ to $CH_4$ at Cu electrodes based on Density Functional Theory (DFT) and Computational Hydrogen Electrode (CHE) models applied to Hori's experimental data.[44] In that work, the authors indicate that the carbon atom of CO adsorbates may be hydrogenated via proton transfer to form HCO at –0.74 V (RHE). Hydrogenation of an adsorbed CO species is proposed to occur directly via proton addition from solution since their availability is significantly greater than hydrogenation from

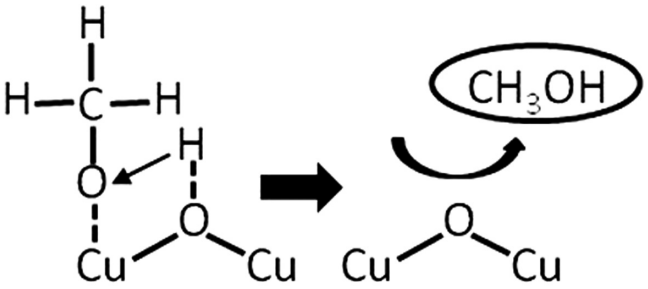


**Figure 8.** Hydrogenation of methoxy adsorbates at $Cu_2O$ (111) surfaces.

adsorbed hydrogen. Accordingly, once the HCO species is formed, the carbon atom continues proton and electron transfer reactions to form $H_3CO$ adsorbates. Following this pathway, the last proton transfer to the $H_3CO$ species (on Cu (211) surfaces) favors $CH_4$ formation by 0.27 eV. In the case of cuprous oxide electrodes as described here, the reduction reaction may benefit from both improved intermediate stability and the ability of $H^+$ species coordinated with surface bound oxygen. This surface would allow hydrogen addition to the oxygen atom of the $H_3CO$ adsorbate rather than the carbon atom as shown in Fig. 8.

While these results show copper oxides are reduced along with $CO_2$, it is interesting to consider Cu(I) stability relative to photoelectrochemical or hydrogenation conditions. In contrast with $CH_3OH$ generation via electrochemical reduction processes where oxidation and reduction reactions are spatially separated, photoelectrochemical and hydrogenation reactions may benefit from relatively stable Cu(I) species. In fact, the photoelectrochemical process with Cu-loaded titania may follow a similar mechanism as the electrochemical case; however, there is no net charge difference at the electrode and the titania may help maintain Cu in the Cu(I) state. Likewise, the water and zinc oxides used in hydrogenation reactions may help promote stable Cu(I) species and reaction intermediates while allowing hydrogenation of oxygen atoms by adsorbed hydrogen as described in the model by Peterson.

## Conclusions

Direct reduction of $CO_2$ to $CH_3OH$ at electrodeposited cuprous oxide thin films is demonstrated at rates up to 43 μmol $cm^{-2}$ $h^{-1}$ and Faradaic efficiencies up to 38%. These rates and efficiencies are remarkably higher than either air-oxidized or anodized Cu electrodes prepared in this study and suggests Cu(I) species may play a critical role in electrode activity and selectivity to $CH_3OH$. Surface analysis of the oxides before and after the reaction show mixed oxidation states ($Cu_2O$, $Cu_4O_3$, and CuO) depending on the method of preparation and $CH_3OH$ yields qualitatively follow Cu(I) concentrations. Experimental results also indicate $CH_3OH$ yields are dynamic and copper oxides are reduced to metallic Cu in a simultaneous process at the potentials required for $CO_2$ reduction. In contrast with Cu electrodes, where $CH_4$ is the preferred reduction product, Cu(I) species may improve the stability of intermediates and alter selectivity towards $CH_3OH$ by enabling hydrogenation of oxygen atoms from $H_3CO$ adsorbates. While more experimental and computational work is needed, these results suggest Cu(I) species may play a critical role in selectivity towards $CH_3OH$ and their stability may be a key factor for maintaining catalytic activity in other (photoelectrochemical or hydrogenation) methanol generation reactions.

## Acknowledgments

This material is based upon work supported as part of the Center for Atomic Level Catalyst Design, an Energy Frontier Research Center funded by the U.S. Department of Energy, Office of Science, Office of Basic Energy Sciences under Award Number DE-SC0001058.

*Louisiana State University assisted in meeting the publication costs of this article.*

## References

1. M. Jayamurthy and S. Vasudevan, *Catal. Lett.*, **36**, 111 (1995).
2. S. Lee, M. Gogate, and C. J. Kulik, *Fuel Sci. & Tech. Int.*, **13**, 1039 (1995).
3. O. Joo, K. Jung, I. Moon, A. Y. Rozovskii, G. I. Lin, S. Han, and S. Uhm, *Ind. Eng. Chem. Res.*, **38**, 1808 (1999).
4. X. M. Liu, G. Q. Lu, Z. F. Yan, and J. Beltramini, *J. Ind. Eng. Chem. Res.*, **42**, 6518 (2003).
5. G. C. Chinchen, K. C. Wangh, and D. A. Whan, *Appl. Catal.*, **25**, 101 (1986).
6. G. C. Chinchen, M. S. Spencer, K. C. Waugh, and D. A. Whan, *J. Chem. Soc. Faraday Trans.*, **83**, 2193 (1987).
7. M. Saito and K. Muruta, *Catal. Surv. Asia*, **8**, 285 (2004).
8. J. Wu, M. Saito, M. Takeuchi, and T. Watanabe, *Appl. Catal. A: Gen.*, **218**, 235 (2001).
9. Y. Hori, *Modern Aspects of Electrochemistry*, Vol. 42, p. 89, Springer, New York (2008).
10. D. Canfield and K. W. Frese, Jr. *J. Electrochem. Soc.*, **130**, 1772 (1983).
11. D. P. Summers, S. Leach, and K. W. Frese, Jr. *J. Electroanal. Chem. Interfacial Electrochem.*, **205**, 219 (1986).
12. K. W. Frese, Jr. and S. Leach, *J. Electrochem. Soc.*, **132**, 259 (1985).
13. A. Bandi, *J. Electrochem. Soc.*, **137**, 2157 (1990).
14. J. P. Popic, M. L. Avramov-Ivic, and N. B. Vukovic, *J. Electroanal. Chem.*, **421**, 105 (1997).
15. N. Spataru, K. Tokuhiro, C. Terashima, T. N. Rao, and A. Fujishima, *J. Appl. Electrochem.*, **33**, 1205 (2003).
16. J. Qu, X. Zhang, Y. Wang, and C. Xie, *Electrochim. Acta*, **50**, 3576 (2005).
17. K. W. Frese, Jr., *J. Electrochem. Soc.*, **138**, 3338 (1991).
18. N. Gupta, M. Gattrell, and B. Macdougall, *J. Electroanal. Chem.*, **594**, 1 (2006).
19. Y. Hori, K. Kikuchi, and S. Suzuki, *Chem. Lett.*, 1695 (1985).
20. M. Azuma, K. Hashimoto, M. W. Hiramoto, M. Watanabe, and T. Sakata, *J. Electrochem. Soc.*, **137**, 1772 (1990).
21. Y. Hori, A. Murata, and R. Takahashi, *J. Chem. Soc. Faraday Trans.*, **85**, 2309 (1989).
22. J. J. Kim, D. P. Summers, and K. W. Frese, Jr., *J. Electroanal. Chem.*, **245**, 223 (1988).
23. Y. Hori, H. Wakebe, T. Tsukamoto, and O. Koga, *Electrochim. Acta*, **39**, 1833 (1994).
24. Y. Hori, I. Takahashi, O. Koga, and N. Hoshi, *J. Mol. Catal. A*, **199**, 39 (2003).
25. Y. Hori, A. Murata, and Y. Yuzuru, *J. Chem. Soc. Faraday Trans.*, **87**, 125 (1991).
26. I. H. Tseng, W. C. Chang, and J. C. S. Wu, *Appl. Catal.. B: Environ.*, **37**, 37 (2002).
27. J. C. S. Wu, H. M. Lin, and C. L. Lai, *Appl. Catal. A: Gen.*, **296**, 194 (2005).
28. Slamet, H. W. Nasution, E. Purnama, K. Riyani, and J. Gunlazuardi, *World Appl. Sci. J.*, **6**, 112 (2009).
29. H. Nakatsuji and Z. Hu, *Int. J. Quantum Chem.*, **77**, 341 (2000).
30. T. Fujitani and J. Nakamura, *Appl. Catal. A: Gen.*, **191**, 111 (2000).
31. Y. Yang, J. Evans, J. A. Rodriguez, M. G. White, and P. Liu, *Phys. Chem. Chem. Phys.*, **12**, 9909 (2010).
32. T. D. Golden, M. G. Shumsky, Y. Zhou, R. A. VanderWerf, R. A. Van Leeuwen, and J. A. Switzer, *Chem. Mater.*, **8**, 2499 (1996).
33. T. Mahalingam, J. S. P. Chitra, S. Rajendran, and P. J. Sebastian, *Semicond. Sci. Technol.*, **17**, 565 (2002).
34. Y. Hori, J. Konishi, T. Futamura, A. Murata, O. Koga, H. Sakurai, and K. Oguma, *Electrochim. Acta*, **50**, 5354 (2005).
35. T. Schedel-Niedrig, T. Neisius, I. Böttger, E. Kitzelmann, G. Weinberg, D. Demuth, and R. Schlogl, *Phys. Chem. Chem. Phys.*, **2**, 2407 (2000).
36. J. Szanyi and D. W. Goodman, *Catal. Lett.*, **10**, 383 (1991).
37. G. R. Sheffer and T. S. King, *J. Catal.*, **115**, 376 (1989).
38. S. Bailey, G. F. Fronment, J. W. Snoeck, and K. C. Waugh, *Catal. Lett.*, **30**, 99 (1995).
39. R. G. Herman, K. Klier, G. W. Simmons, B. P. Finn, and J. B. Bulko, *J. Catal.*, **56**, 407 (1979).
40. J. Nakamura, Y. Choi, and T. Fujitani, *Top. Catal.*, **22**, 277 (2003).
41. M. Sahibzada, I. S. Metcalfe, and D. Chadwick, *J. Catal.*, **174**, 111 (1998).
42. K. Ozawa, Y. Oba, and K. Edamoto, *Surf. Sci.*, **601**, 3125 (2007).
43. D. F. Cox and K. H. Schulz, *J. Vac. Sci. Technol. A*, **8**, 2599 (1990).
44. A. A. Peterson, F. Abild-Pedersen, F. Studt, J. Rossmeisl, and J. K. Norskov, *Energy Environ. Sci.*, **3**, 1311 (2010).